AIMS Biophysics, 3(2): 261-285.
DOI: 10.3934/biophy.2016.2.261
Received: 19 April 2016
Accepted: 20 May 2016
Published: 23 May 2016

http://www.aimspress.com/journal/biophysics

Research article

Microtubule modification influences cellular response to amyloid-β exposure

Nicole Shamitko-Klingensmith [1], Jonathan W. Boyd [1], and Justin Legleiter [1,2,3,*]

[1] The C. Eugene Bennett Department of Chemistry, 217 Clark Hall, West Virginia University, Morgantown, WV 26506, USA
[2] Centers for Neuroscience, Robert C. Byrd Health Sciences Center, PO Box 9304, West Virginia University, Morgantown, WV 26506, USA
[3] NanoSAFE, PO Box 6223, West Virginia University, Morgantown, WV 26506, USA

* **Correspondence:** Email: Justin.legleiter@mail.wvu.edu; Tel: +1-304-293-0175; Fax: +1-304-293-4904.

Abstract: During the normal aging process, cytoskeletal changes such as a reduction in density or disruption of cytoskeletal components occur that can affect neuronal function. As aging is the biggest risk factor for Alzheimer's disease (AD), this study sought to determine how microtubule (MT) modification influences cellular response upon exposure to β-amyloid1-42 (Aβ1-42), which is implicated in AD. The MT networks of hypothalamic GT1-7 neurons were modified by common disrupting or stabilizing drugs, and then the physical and mechanical properties of the modified neurons were determined. The MT modified neurons were then exposed to Aβ1-42 and the ability of the neurons to cope with this exposure was determined by a variety of biochemical assays. Flow cytometry studies indicated that MT disruption reduced the binding of Aβ1-42 to the plasma membrane by 45% per cell compared to neurons with stabilized or unaltered MTs. Although the cells with disrupted MTs experienced less peptide-membrane binding, they experienced similar or increased levels of cytotoxicity caused by the Aβ1-42 exposure. In contrast, MT stabilization delayed toxicity caused by Aβ1-42. These results demonstrate that MT modification significantly influences the ability of neurons to cope with toxicity induced by Aβ1-42.

Keywords: Alzheimer's disease; β-amyloid; microtubules; cellular mechanics; neurodegeneration; protein aggregation

1. Introduction

The cytoskeleton plays a critical role in the complex morphology of neurons, intra- and intercellular signaling, and organelle transport [1]. In neurons, there are three major cytoskeletal components, neurofilaments, actin, and microtubules [2]. Neurofilaments (NFs) are found within the axon and dendrites, where they provide structural support, aid in axonal transport, and regulate axon diameter [3,4]. The inner plasma membrane of neurons is lined with short fragments of filamentous actin (F-actin), while the dendrites and synaptic terminals are rich in F-actin bundles and lattices [1]. Lastly, microtubules (MTs) span the length of the axon and protrude into the base of dendrites, where they provide structural support, and function as tracks for organelle transport [5]. Importantly, each of these cytoskeletal components experience dysfunction with aging that can alter cellular functioning [2,6–12].

There are many examples of age-related microtubule modification throughout the body [10,13–16]. In neurons, exposure to the lipid peroxidation product 4-hydroxy-2(E)-nonenal (HNE, a common product of age-related oxidative stress) causes extensive MT disruption, and HNE adduction with tubulin prevented polymerization [17]. In human studies, tissue biopsied from cognitively healthy adults show an age-dependent decrease in the microtubule density of pyramidal neurons [18]. Together, these findings demonstrate that neuronal MTs are critically affected during aging. This may have implications for the development of Alzheimer's disease (AD), as AD brains display a significant reduction in pyramidal neuron density [19]. MT modification is associated with mitochondrial abnormalities [20,21], and reduced axonal transport resulting from MT disruption could also contribute to the loss of synaptic connectivity between neurons that causes cognitive impairments in AD [18,22]. Considering that aging is the major risk factor for AD [23], it would be beneficial to gain a more complete understanding of how age-related MT modification in neurons may contribute to disease.

Two pathological hallmarks of AD are extracellular plaques of amyloid-β (Aβ) and intraneuronal neurofibrillary tangles (NFTs) containing the hyperphosphorylated microtubule-associated protein Tau (Tau) [24]. Aβ is a 38-43 amino acid long residue that is produced from sequential cleavages of the amyloid precursor protein (APP) [25], but Aβ1-40 and Aβ1-42 are the most abundant forms. Aβ aggregates themselves are toxic, but their presence is also thought to trigger a cascade of events leading to the formation of NFTs [25–27], which ultimately causes the deterioration of the neuronal processes and cell death [28–33].

In the brains of AD individuals, age-related neuronal modifications are amplified in selectively vulnerable regions of the brain, such as the hippocampus and closely related limbic and cortical structures [23,34,35]. These changes can contribute to the increased production or decreased clearance of Aβ, resulting in Aβ-induced neurotoxicity [23]. Specifically, impaired axonal transport, a consequence of age-related MT disruption, has been shown to stimulate the production and accumulation of Aβ [36]. Therefore, although it is well known that Aβ has downstream effects on Tau and subsequently MT stability, age-related MT disruption may actually be a causative factor in AD. Due to the relationship between aging, Aβ, and AD, we sought to determine how microtubule modification influences the cellular response to toxicity caused by aggregates of Aβ1-42. To accomplish this goal, GT1-7 neurons were treated with a variety of MT stabilizing or destabilizing agents, and toxicity associated with exposure to Aβ1-42 aggregates was examined. This work provides insight into how MT modification, which is a common feature of the natural aging process,

may contribute to the development of AD.

2. Materials and Methods

2.1. Cell Culture

GT1-7 hypothalamic neurons were obtained from Dr. Susan Mayo at the University of California, San Diego. Neurons were grown in DMEM medium supplemented with 4.5 g/L glucose, 110 mg/L sodium pyruvate, 1% penicillin-streptomycin (stabilized with 10,000 units penicillin and 10 mg streptomycin/mL), 2 g/L sodium bicarbonate, 584 mg/L L-glutamine (Sigma-Aldrich, St. Louis, MO), 5 mM HEPES (Fisher BioReagents, Waltham, MA) and 10% HyClone® fetal bovine serum (Thermo Scientific, Waltham, MA) [37–41]. Cultures were maintained at 37 °C and 5% CO_2. For all cell-based experiments, serum concentration was reduced to 5%.

2.2. Microtubule treatments and Aβ1-42 Preparation

Colchicine, nocodazole, and paclitaxel (Fisher Scientific) were dissolved in dimethyl sulfoxide (DMSO, Fisher Scientific) and further diluted in the appropriate buffer or medium to a final concentration of 0.1–10 μM. Neurons were exposed to a microtubule (MT) modifier for 4 hours prior to Aβ exposure to ensure cytoskeletal modification. Aβ peptides (Aβ1-42 and FAM-labeled Aβ1-42) were purchased from AnaSpec Inc., Fremont, CA. Lyophilized peptides were stored at −20 °C and allowed to equilibrate to room temperature for 30 minutes before resuspension in 1,1,1,3,3,3-hexafluoro-2-propanol (HFIP, Fisher Scientific) to 1 mM. The peptide solution was sonicated for 10 minutes at room temperature and aliquoted into microcentrifuge tubes. The solution was dried and the peptide films were stored at −20 °C until use. Directly before use, HFIP-treated peptide films were dissolved in DMSO by pipette mixing, vortexing, and sonication for 10 minutes at 37 °C [42]. Peptide solutions were then diluted into the appropriate buffer or medium to a final concentration of 5 μM. DMSO exposure to cells never exceeded 1%.

2.3. Cellular mechanical evaluation via AFM

Cells were seeded on poly-D-lysine coated glass coverslips and allowed to incubate overnight. Neurons were treated with a MT-altering drug or vehicle for 4 hours and then exposed to Aβ for 30 minutes. Cells were washed and fixed in a glutaraldehyde solution [43]. Coverslips were mounted onto the AFM stage and imaged in buffer with a NanoScope V MultiMode scanning probe microscope (Veeco, Santa Barbara, CA) equipped with a closed-loop vertical engage J-scanner. Experiments were conducted in contact and force volume imaging modes. All images were acquired using a VISTAprobe contact mode short cantilever (Nanoscience Instruments, Inc., Phoenix, AZ), where the tip radius was 10 nm and the spring constant was calculated via the thermal tuning method [38,44]. The same probe was used for all results presented. Scan speed for topography images was 0.5 Hz with a pixel resolution of 512 × 512. Force curves were acquired at 10 Hz, and force volume images had a resolution of 128 × 128 curves. Young's modulus (E) was evaluated using NanoScope Analysis software v1.5 (Bruker, Santa Barbara, CA). A Hertz model was applied to determine E, where Poisson's ratio was $\nu = 0.5$ [37,43]. A minimum of 9 cells were evaluated for each sample. E

values were extracted from both the soma and processes. Histograms were produced in MATLAB (Math Works Inc., Natick, MA) and values are given as mean ± standard deviation. Statistical significance was analyzed using an unpaired t-test, where a difference at $p < 0.05$ was considered statistically significant. The soma region of the cell was determined from corresponding topography images by finding the tallest pixel within the cell body and defining a sampling zone where the height of the cell remained within 20% of the height of this tallest pixel. Care was taken to make sure that the coverslips on which the cells were attached remained fully hydrated during mounting to the AFM.

2.4. Assessment of $A\beta_{1-42}$ aggregation state

To determine the Aβ aggregate morphology, Aβ was prepared as described above and diluted in PBS to 5 μM. The solution was spotted onto freshly cleaved mica after 0, 24, and 48 hours of incubation at 37 °C. Mica was rinsed with ultrapure water and immediately dried under a gentle stream of nitrogen. Ex situ images were acquired via tapping mode AFM with a VISTAprobe silicon cantilever with a nominal spring constant of 40 N/m and a resonance frequency of ~300 kHz. AFM image analysis was performed using the image processing toolbox of Matlab, as previously described [45]. The images were imported into Matlab and flattened to correct for background curvature. Using a height threshold, a binary map of the surface was created to locate individual aggregates and by implementing pattern recognition algorithms to the binary map, aggregate features were measured (height, volume, etc.).

The SensoLyte® Thioflavin T (ThT) Aβ aggregation kit (AnaSpec, Fremont, CA) was used to confirm the absence of fibrillar aggregates in the 5 μM Aβ solution over a 48 hour period. 5 μM Aβ was prepared as earlier described and added to an untreated 96 well plate containing a ThT solution. Pretreated Aβ from the supplier that is known to rapidly form fibrils was prepared as recommended and used as a positive control. The fluorescence intensity was monitored via an Infinite M1000 Pro microplate reader (Tecan US, Raleigh, NC) at Ex/Em of 440/484 nm every 10 minutes over 48 hours at 37 °C with no shaking to mimic assay conditions.

2.5. Flow cytometry

Neurons were seeded in 6-well plates and allowed to incubate overnight. A 4 hour MT or vehicle treatment was followed by an 80 minute exposure to FAM-Aβ [46,47]. Samples were thoroughly washed to remove any unbound peptide and they were lifted from the surface using a 0.25% trypsin solution. Neurons were then rinsed and resuspended in cold sorting buffer (1x D-PBS, 25 mM HEPES at pH 7.0, 2.5 mM EDTA, and 1% bovine serum albumin). The fluorescence intensity per cell was assessed with a BD FACSCalibur cytometer and BD FACSDiva v8.0 software (BD Biosciences, Franklin Lakes, NJ).

2.6. Plasma membrane degradation assay

Neurons were seeded at 10,000 cells/100 μL medium on a tissue culture-treated 96-well plate and allowed to incubate for 24 hours. Cells received a MT modifying pretreatment, followed by an Aβ exposure for an additional 24 or 48 hours. Ethidium homodimer-1 (EthD-1, Molecular Probes,

Grand Island, NY) was used to evaluate plasma membrane degradation according to the manufacturer's protocol. EthD-1 enters neurons with compromised membranes to produce a bright red fluorescence upon binding to nucleic acids. As a control, a group of vehicle-treated cells received a treatment with 70% methanol 30 minutes prior to EthD-1 exposure. A 6 μM stock of EthD-1 was prepared in Dulbecco's phosphate buffered saline (D-PBS, Fisher Scientific) and 100 μL was added to each well for a final concentration of 3 μM. The samples were incubated for 45 minutes at room temperature and the fluorescence intensity was measured at Ex/Em of 495/635 nm. All assay measurements were performed at least in triplicate.

2.7. MTT reduction assay

Samples were prepared exactly as described for the plasma membrane degradation assay, and MTT reduction was evaluated via the MTT assay kit (Abnova, Walnut, CA). The MTT assay involves the conversion of MTT (3-(4,5-dimethylthiazol-2-yl)-2,5-diphenyltetrazolium bromide) to insoluble formazan crystals. The tetrazolium salt MTT reduction is dependent on reducing agents, NADH and NADPH, produced by metabolically active cells. MTT reagent was added to each well according to the manufacturer's protocol and the samples were incubated for 4 hours at 37 °C. The crystals were solubilized by adding 100 μL of the provided buffer solution to each well with gentle shaking for 1 hour at room temperature. The absorbance was measured at 570 nm.

2.8. Statistical analysis

Plasma membrane degradation and MTT reduction was analyzed using GraphPad Prism v5 software (GraphPad Software Inc., La Jolla, CA). Statistical significance was determined using a one-way analysis of variance (ANOVA) with Turkey's multiple comparison test. Differences at $p < 0.05$ were considered statistically significant. All assay data is plotted as a ratio of value/baseline (vehicle control) where error bars reflect standard error of the mean.

3. Results

3.1. Microtubule modification alters the physical and mechanical properties of neurons

To determine how the MT network influences the ability of Aβ1-42 aggregates to cause toxicity, it was first necessary to induce MT modification by common disrupting or stabilizing treatments. Hypothalamic GT1-7 neurons were treated with a MT disruptor (colchicine or nocodazole) or stabilizer (paclitaxel) for four hours at 0.1, 1.0, and 10.0 μM. Both colchicine and nocodazole cause MT depolymerization at high concentrations [48], while paclitaxel mechanically stabilizes MTs by binding to β-tubulin [49]. After four hours of treatment, the physical and mechanical properties of the neurons were examined. Neurons with chemically disrupted MTs displayed morphological changes, specifically in reducing extensions of the plasma membrane that are commonly considered to model neurites in the GT1-7 cell line (Figure 1). This observation is in agreement with other studies that reported MT disruption induced morphological alterations in the periphery of PC-12 and endothelial cells [50–52]. Cells treated with paclitaxel did not display a reduction in extensions of the plasma membrane, as would be expected with stabilization of MTs.

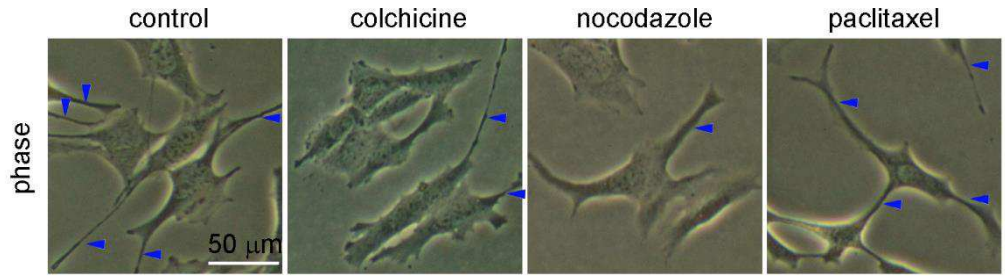

Figure 1. Morphological changes of GT1-7 neurons treated with MT modifiers. Neurons were exposed to the vehicle, a MT-depolymerizers (colchicine and nocodazole), or a MT-stabilizer (paclitaxel) for 4 hours. Phase contrast microscopy images reveal morphological differences in live neurons with the various treatments. Blue arrows indicate the presence of extensions of the plasma membrane.

To determine the mechanical impact of MT modification, the Young's modulus (E, a measure of stiffness) of individual neurons was mapped by AFM-based force volume imaging (Figure 2A). After four hours of treatment with a MT-modifier, neurons were fixed with glutaraldehyde to effectively preserve cell surface features [53]. Fixation was necessary due to instrumental limitations, i.e., the length of time required to produce a force map, but it is common practice for AFM-based cellular experiments, as it improves image resolution and consistency in mechanical measurements [43,54–61]. Fixation is known to increase cellular stiffness [43,54]; therefore, these studies reflect the relative changes in E. That is, the values of E reported in this study are not biologically accurate, but fixation allows for fair comparisons of stiffness across samples whereas the properties of living cells may change during the mapping process. Relative values of E were determined by extracting individual force-distance curves from the mechanical surface maps. Curves were selected from two neuronal regions, the soma and the extended processes, to produce E histograms for each sample (Figure 2B-C). Histograms represent E data extracted from a minimum of 9 neurons for each treatment.

Treatment with 10 μM colchicine for four hours significantly decreased E in the somatic region by 31% (Figure 2B). Literature reports on the mechanical effect of colchicine are conflicting. For instance, neutrophils treated with similar concentrations of colchicine experienced significant stiffening [62]. In NRK fibroblasts, however, no mechanical alteration or change in stress fibers was observed after treatment with 100 μM colchicine [63]. Furthermore, vascular smooth muscle cells exhibited a significant decrease in cell stiffness when treated with colchicine [64]. Thus, the influence of colchicine on cellular mechanics is highly dependent on cell type, the state of cell division, and even on the region of the cell. Unlike the somatic region, after colchicine treatment the rigidity of the neuronal processes was not significantly different than that of the vehicle-treated control (1.8% difference). The effect of softening in the somatic region while retaining stiffness in the processes can be related to previous studies on fibroblasts. When aged hamster fibroblasts were treated with a microtubule disruptor, centrifugal depolymerization occurred and MT remnants were found in the cortical areas [14]. The reasoning for this effect is unknown and could be attributed to several factors (aging may disrupt the centrosome, reverse the polarity of MTs, alter the stability of the anchorage to the membrane, etc.) [14].

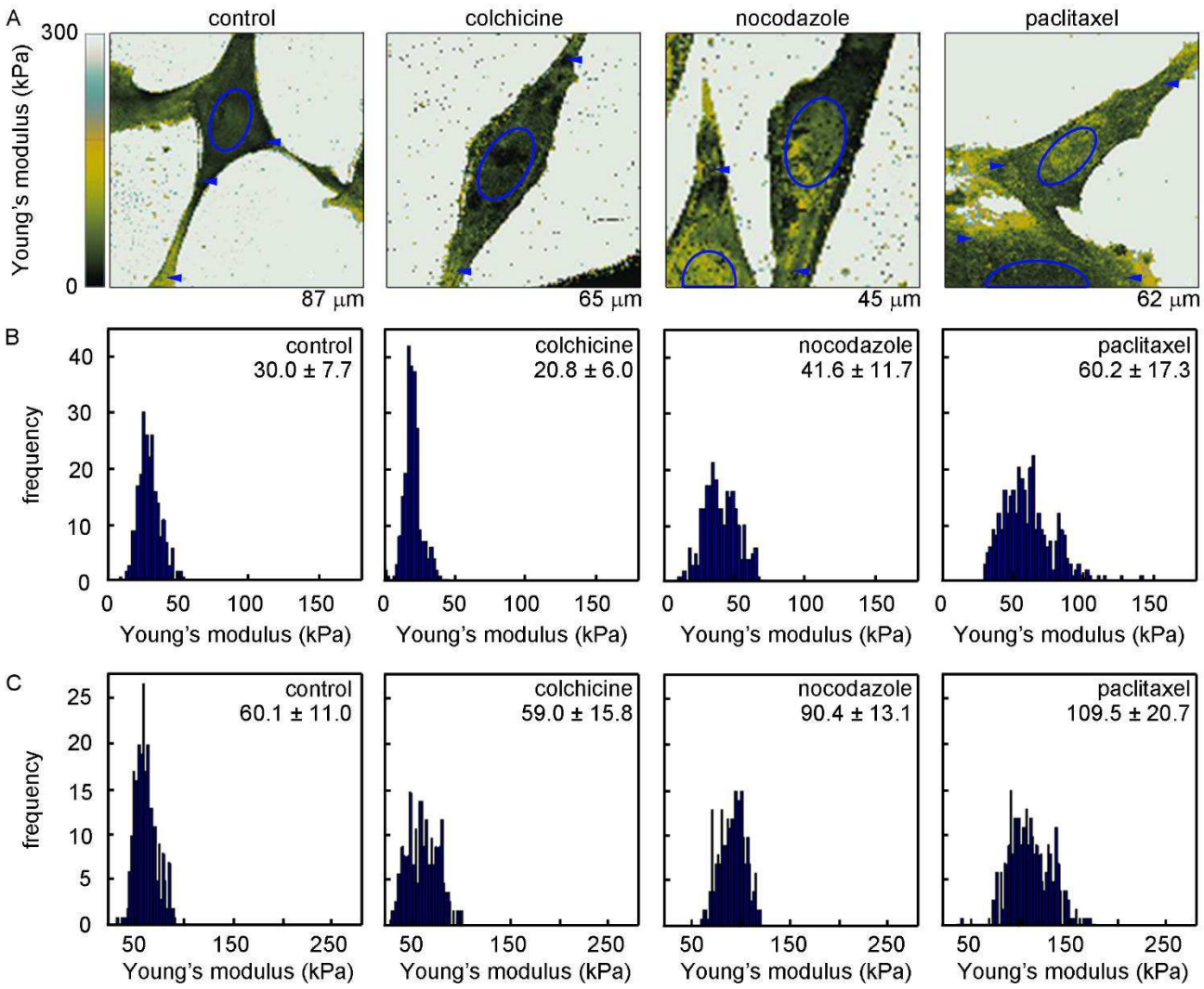

Figure 2. Measuring the Young's modulus of neurons treated with MT modifiers. (a) Examples of Young's modulus (E) maps obtained by force volume imaging. Histograms of the average value of E were constructed by extracting values from the (b) soma or (c) processes of neurons treated with: the vehicle or MT-altering drug (colchicine, nocodazole, paclitaxel) for 4 hours. Measurements represent the mean E ± standard deviation. The ellipses represent regions from which the soma measurements were sampled and the arrows indicate where measurements of the processes were sampled.

Unlike colchicine, when cells were treated with 10 μM nocodazole, the stiffness of the soma and processes increased by 39% and 50%, respectively, as compared to the vehicle-treated control (Figure 2B-C). This is in agreement with findings from similar studies on L929 fibroblast-like cells where an increase in cellular stiffness was observed after treatment with nocodazole [65]. This was attributed to the reorganization of the cytoskeletal network after MT depolymerization. Cytoskeletal reorganization after injury was observed in Swiss 3T3 cells; when cells were treated with MT disruptors, actin polymerization occurred in a dose- and time-dependent manner [66]. These findings demonstrate that cell stiffening after nocodazole-induced MT disruption is a consequence of actin polymerization. The discrepancy in mechanical changes between colchicine and nocodazole treated

neurons may arise from the binding mechanisms to tubulin. Although nocodazole binds tubulin more rapidly than colchicine, colchicine binding is irreversible [67], which may explain the variation in cellular stiffness between the two treatments.

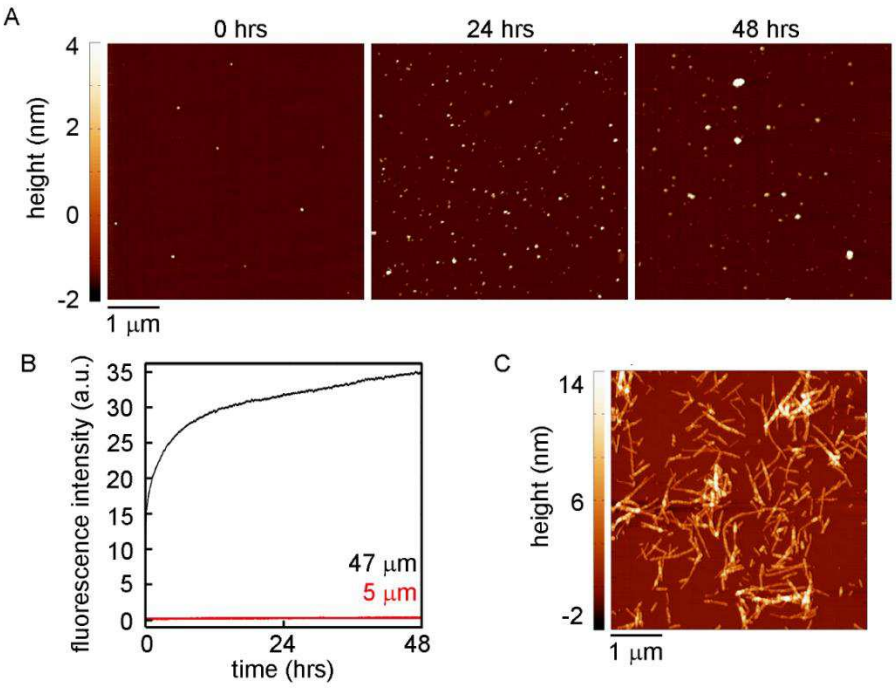

Figure 3. Assessment of the Aβ1-42 aggregation state. (a) Oligomeric aggregates were observed when 5 μM Aβ1-42 was spotted onto freshly cleaved mica and analyzed via ex situ AFM imaging after 0, 24 or 48 hours of incubation at 37 °C in a physiologically relevant buffer. (b) The thioflavin T assay was performed to detect the presence of β-sheet, a characteristic of fibrils. The red line corresponds to 5 μM Aβ which was prepared as described in the methods section, and the black line represents 47 μM Aβ1-42 obtained from the SensoLyte® Aggregation kit and prepared as recommended by the manufacturer. (c) Fibrillar aggregates were observed when 47 μM Aβ1-42 was imaged via ex situ AFM after 48 hours of incubation.

When neurons were treated with 10 μM paclitaxel, rigidity increased by 101% and 89% in the somatic region and the processes, respectively, compared to the vehicle-treated control sample (Figure 2B-C). Our results are consistent with a similar study, in which cellular stiffening occurred in cortical neurons when treated with 10 μM paclitaxel [68]. Although other studies have demonstrated that MT-disruption may produce an increase in cellular stiffness by activating a secondary response of actin polymerization, paclitaxel-mediated MT stabilization was not reported to stimulate actin production [66,69]. Therefore, the increase in cellular stiffness is likely due to the mechanical stabilization of the MT network. Taken together, these studies confirmed that a four hour exposure to MT modifiers altered the morphology and the mechanical stiffness of neurons.

3.2. Microtubule disruption reduces Aβ1-42 binding to the cell membrane

Before investigating how MT modification influences Aβ1-42-induced cytotoxicity, it was necessary to characterize aggregation state of Aβ1-42 that the cells would be exposed to in this study. This is critical because the extent of membrane affinity [70,71] and the resulting toxicity [72] is dependent on Aβ aggregation state. A fresh Aβ1-42 solution was prepared from lyophilized peptide using the Stine preparation method [42]. The solution was diluted to 5 μM, and the aggregation state of the peptide was determined by ex situ AFM imaging at 0, 24, and 48 h of incubation (Figure 3A). Over the 48 h incubation, only oligomeric aggregates were observed (even at 0 h of incubation); however, these oligomers increased in number over 24 h. After 24 h, the number of oligomers remained relatively steady. Oligomers increased in size from an average height of 3.0 ± 1.3 nm to 4.2 ± 1.2 nm over the 48 h period as well. The size of Aβ1-42 oligomers can vary considerably depending on the preparation method, but the height is consistent with previously observed large Aβ1-42 oligomers [73–75]. Elongated fibrillar aggregates were not observed in any 5 μM sample within 48 h. The absence of fibrils in the 5 μM solution was confirmed by a Thioflavin T (ThT) fluorescence assay, which is based on the interaction between ThT and β-sheet secondary structure, a characteristic of amyloid fibrils (Figure 3B). As a positive control, ThT assays were performed on a solution of 47 μM Aβ1-42 guaranteed to form fibrils by the manufacturer, and this solution caused an immediate increase in fluorescence intensity, consistent with rapid fibril formation and elongation. Fibril formation within the 47 μM Aβ1-42 solution was confirmed by AFM (Figure 3C). Cells were only exposed to freshly-prepared 5 μM monomeric/oligomeric Aβ1-42 solutions.

It has been demonstrated that cells may exhibit resistance to Aβ-membrane binding based on specific cellular characteristics, such as the presence of apoptotic signaling molecules, cell size, stage of the cell cycle, and cytosolic ATP levels [46]. Specifically, when PC-12 cells or GT1-7 neurons were exposed to FITC-Aβ1-42, the cells could be divided into three distinct subpopulations based on their susceptibility to Aβ binding (those with no binding affinity, high binding affinity, or extra-high binding affinity) [46]. Considering this, we wanted to determine if altered neuronal morphology and mechanical stiffness from MT modification altered the susceptibility of GT1-7 cells to Aβ1-42 binding. GT1-7 cells were pretreated with a MT-modifier or a vehicle control (DMSO) for four hours and then were exposed to 5 μM FAM-Aβ1-42 solution for 80 minutes. The FAM-Aβ1-42 solution contained a mixture of monomer and oligomers, but no fibrils. Pretreatments were not removed from the culture medium during the additional 80 minute incubation to prevent MT recovery. After the 80 minute FAM-Aβ1-42 exposure, aggregate-membrane binding was evaluated by flow cytometry (Figure 4A). Approximately 0.2% of the vehicle-treated control had positive staining, which may be attributed to the natural fluorescence of the living neurons, likely due to flavoproteins that have a similar emission wavelength as FAM-Aβ1-42 (~ 521 nm) [76]. Excluding the vehicle-treated control which received no FAM-Aβ1-42 exposure, the vast majority of the neurons in each sample population had membrane bound FAM-Aβ1-42 (Figure 4A); however, Aβ binding for the entire sample population was slightly lower for neurons pretreated with colchicine (95.2 ± 0.5%, $p < 0.01$ to 0.001) and nocodazole (96.5 ± 0.1%, $p < 0.001$) than those treated with the FAM-Aβ1-42 only (98.4 ± 0.1%). The population of neurons pretreated with paclitaxel experienced a similar level of aggregate-membrane binding (98.5 ± 0.1%, $p > 0.05$) as the FAM-Aβ1-42 control. This contrasts results from the previously mentioned study [46], and the discrepancy between the aggregate-membrane binding is likely due to the peptide preparation technique, as it has been

demonstrated that different aggregate species elicit distinctive membrane interactions [77].

While FAM-Aβ1-42 bound over 95% of cells with or without modified MT networks, the amount of FAM-Aβ1-42 bound per cell was affected by MT modification (Figure 4B). Pretreatment with paclitaxel did not significantly alter the amount of FAM-Aβ1-42 bound per cell compared to control cells with unaltered MT networks; however, neurons pretreated with colchicine and nocodazole were bound by approximately 45% less peptide per cell. This decrease in peptide-membrane binding likely occurred due to the compromised state of neurons with disrupted MT networks. Although the extended processes of the MT disrupted cells were morphologically altered (Figure 1), the reduced amount FAM-Aβ1-42 per cell does not appear to be a consequence of reduced cellular surface area available for binding due to altered cell size and shape associated with MT disruption. The available cellular surface area for cells with unaltered or altered MT networks was estimated by measuring the area occupied by cells using fluorescence microscopy and no statistical difference was observed between treatments.

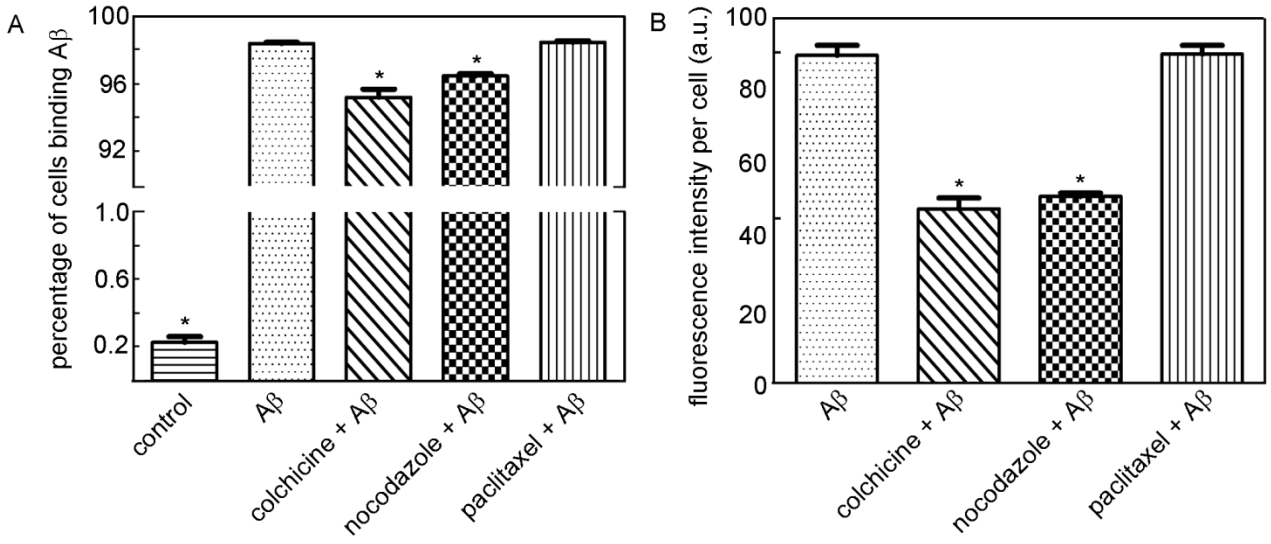

Figure 4. The extent of aggregate-membrane binding determined by flow cytometry. (a) The percentage of cells in each population that had membrane bound Aβ1-42. (b) The amount of aggregate-membrane binding per cell. Neurons were treated with a vehicle or various MT-altering drugs (colchicine, nocodazole, paclitaxel) for 4 hours followed by an 80 minute incubation with FAM-Aβ (with the exception of the vehicle control). Cells were extensively rinsed in physiological buffer to remove any unbound Aβ before analysis. Measurements were made in triplicate, with 20,000 events per sample. Marker (*) represents intensities found to be statistically different ($p < 0.05$) from the Aβ control and error bars represent standard error of the mean (SEM).

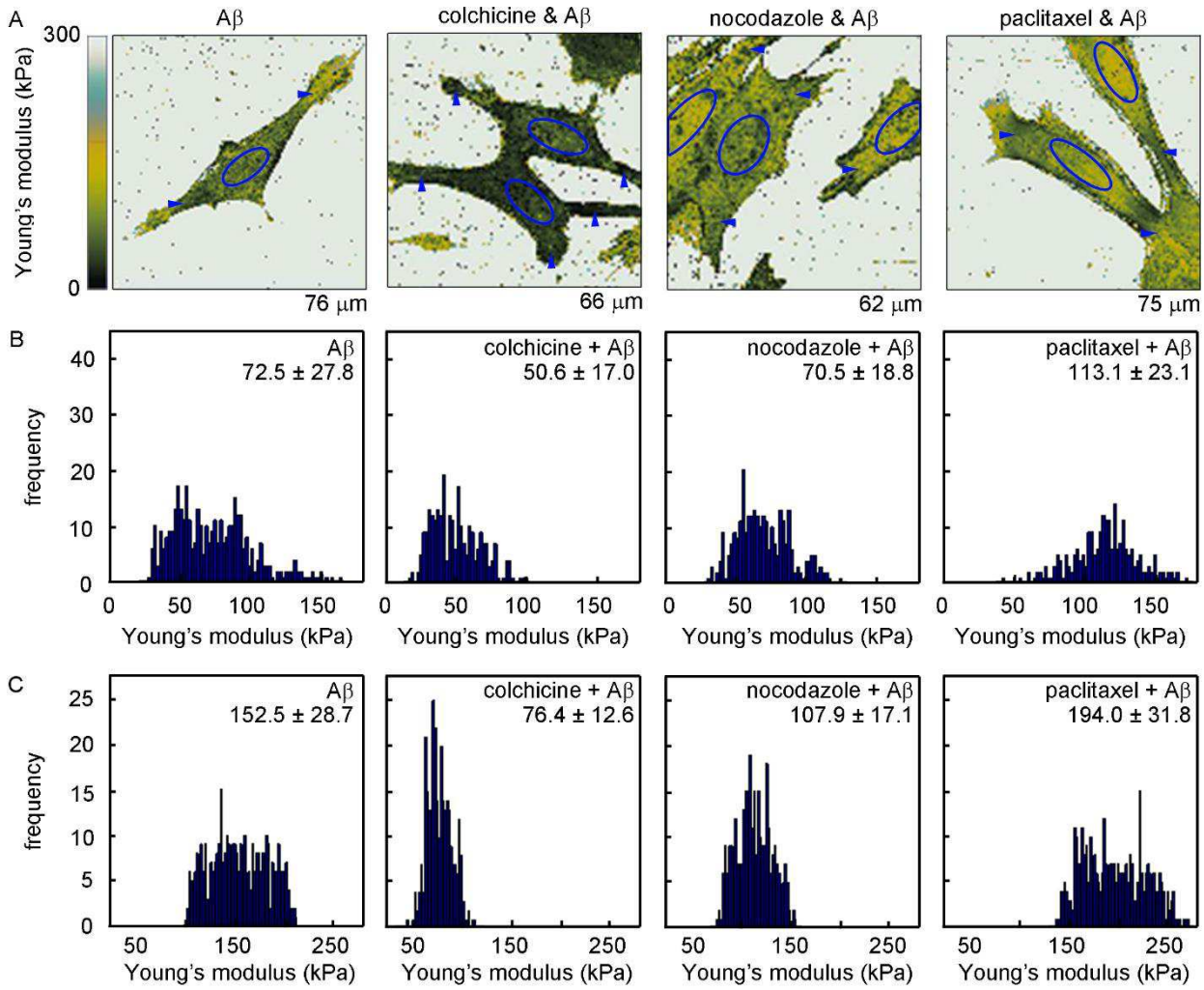

Figure 5. Measuring the Young's modulus of neurons treated with a MT modifier and Aβ1-42. (a) Maps of Young's modulus obtained by force volume imaging. Histograms of the average value of E were constructed by extracting values from the (b) soma or (c) processes of neurons treated with: the vehicle or MT-altering drug (colchicine, nocodazole, paclitaxel) for 4 hours followed by a 30 minute exposure to oligomeric Aβ1-42. Measurements represent the mean E ± standard deviation. The ellipses represent regions from which the soma measurements were sampled and the arrows indicate where measurements of the processes were sampled.

3.3. Exposure to Aβ1-42 alters neuronal rigidity

Numerous studies have demonstrated that Aβ causes membrane disruption, which can lead to structural and functional cellular changes [78–84]. To determine if Aβ1-42 binding affects the mechanical stability of neurons, surface maps of E were produced by force volume imaging. Neurons were pretreated with a MT modifier or vehicle (DMSO) for four hours prior to a 30 minute exposure to fresh preparations of 5 μM Aβ1-42. The preparations of Aβ1-42 consisted of a mixture of monomeric and oligomeric species but did not contain fibrils. Again, the MT modifiers were not removed from the culture medium to prevent MT recovery. For all sample populations, the E of the

soma and processes significantly increased upon Aβ1-42 exposure compared to control cells that were treated similarly in regards to their MT networks but not exposed to Aβ (Figure 5, which can be compared directly with Figure 2, and Table 1). Interestingly, stiffening occurred regardless of the initial state of the MT network at the time of exposure. A similar stiffening effect was reported previously, where an increase in cell stiffness was observed after exposure to 5 μM oligomeric Aβ1-42 solutions for 30 minutes [85].

Table 1. Percent difference in Young's modulus (E) after 30 minute exposure to Aβ1-42.

	Soma (% change)	Processes (% change)
Control	142	154
+ Colchicine	143	29
+ Nocodazole	69	19
+ Paclitaxel	88	77

Percent differences were calculated for both the soma and neuronal processes. E increased significantly in each neuronal region after treatment, with $p < 0.001$

3.4. Microtubule disruption reduces the ability of neurons to cope with Aβ1-42 exposure

Next, we examined the influence of MT disruption on the ability of GT1-7 cells to cope with exposure to Aβ1-42. Plasma membrane (PM) degradation and MTT reduction assays were used, as these assays are effective tools for assessing Aβ-induced toxicity [72,86–90]. Neurons were pretreated with an MT-disruptor (colchicine or nocodazole) or the vehicle (DMSO), at concentrations ranging from 0.1 to 10 μM for 4 hours, and then Aβ1-42 (5 μM final concentration) was added to the culture medium for an additional 24 to 48 hours. Again, the preparations of Aβ1-42 consisted of a mixture of monomeric and oligomeric species but did not contain fibrils. As an important note, the amount of PM degradation or MTT reduction for each sample is plotted relative to the control, i.e., the total amount of PM degradation or MTT reduction for neurons that were treated with only the vehicle (DMSO).

When neurons were exposed to 0.1–10 μM colchicine, there was no statistical difference in the PM degradation induced by the various colchicine concentrations at each respective time point (white bars to the left, Figure 6A). However, when neurons were pretreated with colchicine at each concentration and then exposed to Aβ1-42 for an additional 24 or 48 hours (gray bars in the center), PM degradation significantly increased by 2.25–3.02 times as compared to the neurons that received only a colchicine treatment for 28 or 52 hours. In some cases, neurons with a coexposure to both colchicine and Aβ1-42 (gray bars in the center), experienced 1.30–1.59 times more PM degradation than samples exposed to Aβ1-42 alone (black bars to the right). This demonstrates that MT disruption by colchicine enhances the toxicity of Aβ1-42 aggregates, especially considering that the neurons with disrupted MTs were bound by half as much Aβ compared to neurons without MT disruption as assessed by flow cytometry (Figure 4B).

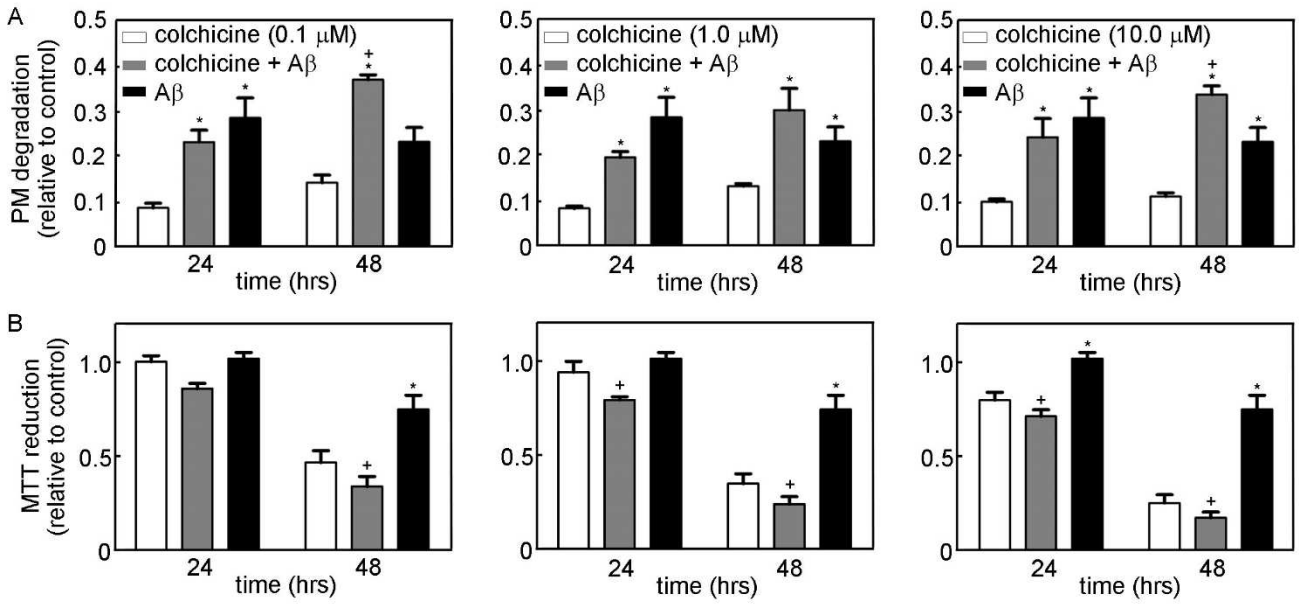

Figure 6. Cellular response to Aβ1-42 after colchicine treatment. (a) PM degradation and (b) MTT reduction was evaluated after neurons were pretreated with the vehicle (DMSO), or MT-destabilizing drug (colchicine) followed by a 24 or 48 hour exposure to 5 μM Aβ. Bars are plotted as relative to the vehicle control (1.0). White bars represent neurons treated with colchicine only, gray bars represent treatment with both colchicine and Aβ1-42, and black bars represent treated with Aβ1-42 only. The concentration of the drug treatment is shown in the legend of (a). The (*) represents samples found to be statistically different from neurons only treated with colchicine, and the (+) indicates samples that are statistically different from the Aβ1-42 exposed control ($p < 0.05$). Error bars represent standard error of the mean (SEM). PM degradation or MTT reduction for each sample is plotted relative to the total amount of PM degradation or MTT reduction for neurons that were treated with only the vehicle (DMSO).

There was little difference in MTT reduction of the neurons exposed to 0.1 μM colchicine, Aβ1-42, or coexposure to both agents after 24 hours of treatment (Figure 6B). However, with exposure to higher concentrations of colchicine (or longer exposures to 0.1 μM colchicine) with or without the presence of Aβ1-42, the MTT response significantly decreased by 22–77% compared to neurons that were exposed only to Aβ1-42. This supports the findings from the plasma membrane degradation study; MT disruption by colchicine reduces neuronal viability, and therefore, the neurons are unable to efficiently cope with even low levels of membrane bound Aβ1-42 as was determined by flow cytometry (Figure 4B).

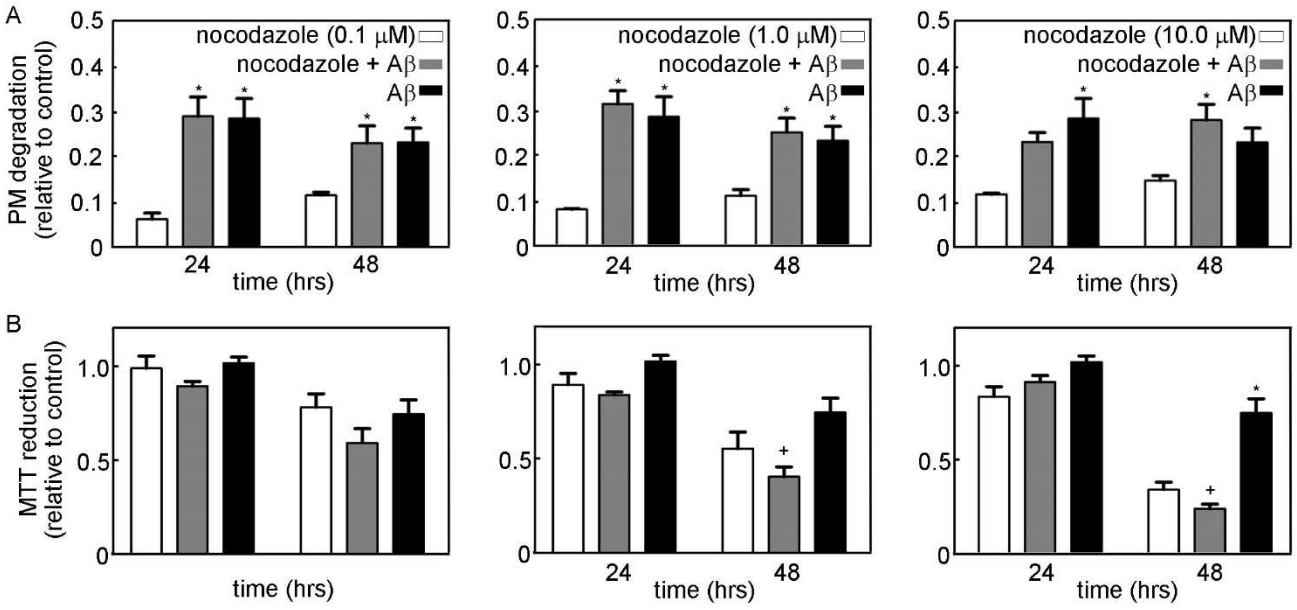

Figure 7. Cellular response to Aβ1-42 after nocodazole treatment. (a) PM degradation and (b) MTT reduction was evaluated after neurons were pretreated with the vehicle (DMSO), or MT-destabilizing drug (nocodazole), followed by a 24 or 48 hour exposure to 5 μM Aβ1-42. Bars are plotted as relative to the vehicle control (1.0). White bars represent neurons treated with nocodazole only, gray bars represent treatment with both nocodazole and Aβ1-42, and black bars represent neurons treated with Aβ1-42 only. The concentration of the drug treatment is shown in the legend of (a). The (*) represents samples found to be statistically different from neurons only treated with nocodazole, and the (+) indicates samples that are statistically different from the Aβ1-42 exposed control ($p < 0.05$). Error bars represent standard error of the mean (SEM). PM degradation or MTT reduction for each sample is plotted relative to the total amount of PM degradation or MTT reduction for neurons that were treated with only the vehicle (DMSO).

Neurons that received treatment with nocodazole experienced slight increases in PM degradation as the concentration increased from 0.1–10.0 μM, but that amount was not statistically different (white bars to the left, Figure 7A). When neurons pretreated with nocodazole for four hours were exposed to Aβ1-42 aggregates for an additional 24 or 48 hours, PM degradation increased significantly by 2.00–4.62 times for cells treated with 0.1 and 1.0 μM nocodazole at 24 and 48 hours, as compared to the neurons receiving only a 0.1 or 1.0 μM nocodazole treatment. Neurons pretreated with 10 μM nocodazole followed by an exposure to Aβ1-42 for an additional 24 hours did not experience a statistically significant increase in PM degradation as compared to those exposed to 10 μM nocodazole alone. This result is likely due to the fact that 10 μM nocodazole itself is considerably more toxic than the lower concentrations of the drug.

Interestingly, the MTT reduction of neurons exposed to nocodazole, Aβ1-42, or a combination thereof for 24 hours was essentially analogous (Figure 7B). After 48 hours of coexposure to 1.0 μM nocodazole and Aβ1-42 (gray bar in the center), MTT response decreased nearly by half, as compared to the neurons treated with Aβ1-42 only (black bars to the right). Considering that neurons

pretreated with nocodazole experienced only half as much aggregate-membrane binding as assessed by flow cytometry (Figure 4B), this indicates that neurons with disrupted MTs had a reduced ability to cope with exposure to toxic Aβ1-42. After 48 hours, treatment with 10 μM nocodazole alone or a combination of nocodazole and Aβ1-42 reduced MTT response by over half of that caused by treatment with only Aβ1-42, indicating that nocodazole itself can cause a large reduction in MTT response at high concentrations.

Overall, nocodazole decreased the ability of GT1-7 cells to cope with exposure to Aβ in a similar fashion as colchicine; however, the toxic effects were less severe in the nocodazole treated samples. This could be attributed to the different binding mechanisms of the MT disruptors to tubulin, which produce distinct mechanical responses, or a reduction in axonal transport and signaling caused by the breakdown of MTs. In any case, the MT disrupted samples treated with Aβ1-42 aggregates experienced just as much, or in some instances, greater toxicity than neurons treated with Aβ1-42 alone, despite having a reduced amount of Aβ directly interacting with the cell (reduced membrane binding, Figure 4B). This result suggests that MT disruption interferes with the cellular response mechanisms to Aβ1-42-mediated toxicity, impairing a cell's ability to efficiently cope with exposure to Aβ1-42.

3.5. Microtubule stabilization delays the onset of Aβ1-42-induced toxicity

Next, we determined the effect of MT stabilization on the ability of GT1-7 cells to cope with exposure to Aβ1-42. Neurons were pretreated with paclitaxel at concentrations ranging from 0.1–10 μM for 4 hours, and then 5 μM Aβ1-42 was added to the culture medium for an additional 24 to 48 hours. The preparations of Aβ1-42 consisted of a mixture of monomeric and oligomeric species but did not contain fibrils. Control cells were treated with the DMSO vehicle prior to exposure to Aβ1-42. Neurons receiving treatment with paclitaxel alone did not experience any statistical difference in PM degradation (white bars to the left, Figure 8A). However, PM degradation significantly increased by 2.88–4.31 times when neurons were pretreated with paclitaxel and then exposed to Aβ1-42 (gray bars in the center). Interestingly, at 24 hours, the PM degradation caused by coexposure to paclitaxel and Aβ1-42 was half of that induced by Aβ1-42 alone (black bars to the right). This effect was lost after 48 hours of treatment. This indicates that MT-stabilization by paclitaxel may be able to delay the onset of cytotoxicity mediated by Aβ1-42.

There was no statistical difference in the MTT reduction of neurons exposed to paclitaxel at 0.1 or 1.0 μM, Aβ1-42, or a combination thereof (Figure 8B). However, the MTT response of neurons treated with 10 μM paclitaxel was 1.30–2.33 times higher than any other population after 24 and 48 hours. This likely occurred because the MT network is highly associated with mitochondrial shape, movement and function [91–94], and its stabilization could promote mitochondrial activity. For example, hyperphosphorylation of Tau, which is a critical component to MT stabilization, inhibited mitochondrial function in PC-12 cells and mouse brain cortical neurons [95]. Thus, it is not unreasonable to observe an increase in MTT response after MT-stabilization. Nevertheless, there was no significant difference in MTT reduction between neurons coexposed to paclitaxel (at all concentrations) and Aβ1-42, or neurons treated with the peptide solution only. Combined with results of the plasma membrane degradation assay, this data suggests that MT-stabilization can improve the cellular response mechanisms ability to cope with the Aβ1-42 exposure, as the amount of Aβ bound per cell treated with paclitaxel was similar to control cells as was assessed by flow cytometry (Figure

4B).

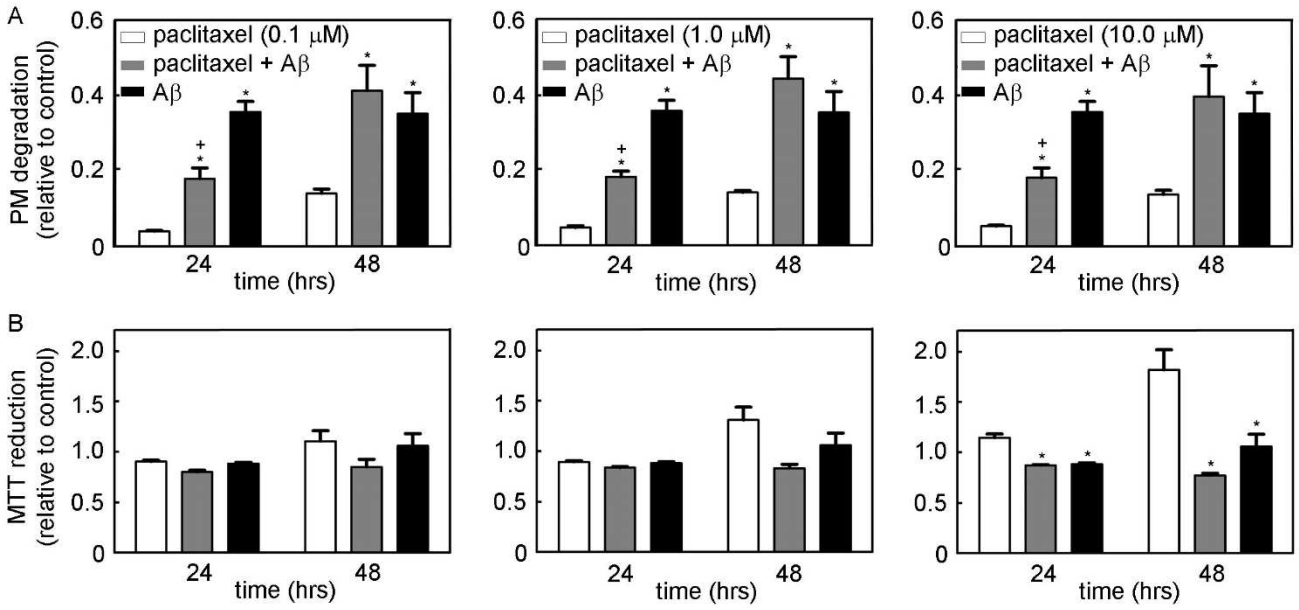

Figure 8. Cellular response to Aβ1-42 after paclitaxel treatment. (a) PM degradation and (b) MTT reduction was evaluated after neurons were pretreated with the vehicle (DMSO), or MT-stabilizing drug (paclitaxel) followed by a 24 or 48 hour exposure to 5 μM Aβ1-42. Bars are plotted as relative to the vehicle control (1.0). White bars represent neurons treated with paclitaxel only, gray bars represent treatment with both paclitaxel and oligomeric Aβ1-42, and black bars represent neurons treated with Aβ1-42 only. The concentration of the drug treatment is shown in the legend of (a). The (*) represents samples found to be statistically different from neurons only treated with paclitaxel, and the (+) indicates samples that are statistically different from the Aβ1-42 exposed control ($p < 0.05$). Error bars represent standard error of the mean (SEM). PM degradation or MTT reduction for each sample is plotted relative to the total amount of PM degradation or MTT reduction for neurons that were treated with only the vehicle (DMSO)

4. Discussion

Our studies sought to determine the role of MT modification on cytotoxicity mediated by Aβ1-42 in a non-fibrillar form. That is, preparations of Aβ1-42 used in this study were mixtures of monomeric and oligomeric forms of the peptide. While the number of oligomers increased over 24 hours, fibrils were not observed in the preparations Aβ1-42 for up to 48 h. The role of MT modifications on cytotoxicity was accomplished by examining the effects of MT disruption and stabilization in GT1-7 neurons exposed to 5 μM Aβ1-42. Although over 95% of neurons in each sample treatment group had membrane bound Aβ1-42, MT disruption by colchicine and nocodazole significantly reduced the extent of Aβ-membrane binding per cell. The reduction of Aβ-membrane binding likely occurred due to the compromised nature of the neurons that received an MT disrupting treatment. Alterations in neuronal rigidity caused by MT alterations did not appear to affect Aβ-membrane binding; specifically, colchicine reduced neuronal rigidity and nocodazole increased

neuronal rigidity compared to neurons with unaltered MTs. This contrasting effect was unexpected, considering that both colchicine and nocodazole cause MT depolymerization at high concentrations [96], but the discrepancy could be due to the differing binding affinities of each drug to tubulin, and/or their mechanisms of action. Literature reports on the tubulin binding site(s) for nocodazole or colchicine are conflicting based on the species which the tubulin was derived from, and experimental designs [67,97–102]; however, a common finding is that nocodazole-tubulin binding is reversible, whereas colchicine-tubulin binding is essentially irreversible [67,96,98,103–105]. Accordingly, the tight binding of colchicine to tubulin likely contributed to the significant softening of the cells, and to the reduced neuronal viability, compared to nocodazole treated neurons. In any case, the reduction in neuronal viability caused by either MT disruptor enhanced the neurotoxicity of Aβ1-42 in a synergistic way. This is supported by the observation that neurons with unaltered MTs had double the amount of membrane bound Aβ per cell as determined by flow cytometry, but experienced similar or decreased levels of PM degradation compared to the neurons with disrupted MT networks (Figure 9). On the contrary, MT stabilization by paclitaxel had a protective effect against Aβ1-42, as there was reduced toxicity after 24 h exposure to Aβ1-42 despite having similar amounts of Aβ bound to the cell (Figure 9).

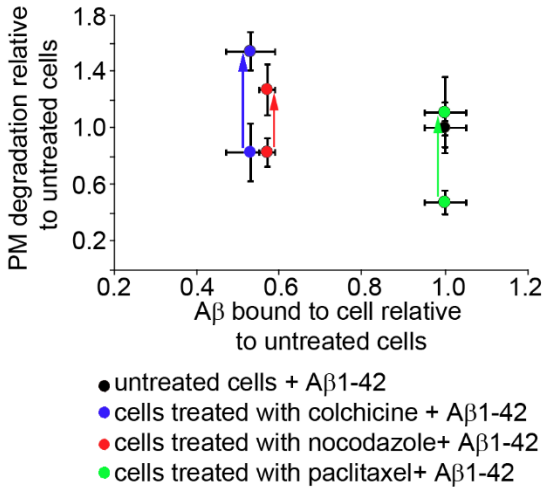

Figure 9. A comparison of the relative PM degradation associated with exposure to Aβ1-42 of cells pretreated with MT altering drugs (10 μM treatment) to cells with no drug treatment to the amount of Aβ bound per cell as measured by flow cytometry. The arrows demonstrate how the relative PM degradation changes from 24 h to 48 h for cells treated with colchicine (blue), nocodazole (red), or paclitaxel (green). As the data is plotted relative to the measurements associated with cells that were not treated with drugs, the position of the untreated cells + Aβ1-42 remains at position (1.0, 1.0).

The protective effect of MT stabilization against Aβ-induced cytotoxicity on primary neuronal cultures has been previously observed [88,106,107]. There, neurons were treated with 0.1 μM paclitaxel for 2 hours before exposure to either 10 μM Aβ1-42 or Aβ25-35. Importantly, the Aβ solutions used in those studies were prepared by incubations at 37 °C for 24 hours in 10 mM Tris-HCl, a preparation technique that is known to produce fibrillar aggregates [42,108]. Furthermore, only peptide solutions with greater than 70% β-sheet conformation were utilized in that study, as

confirmed by circular dichroism [88,106,107]. Taken together, the observations that paclitaxel-mediated MT stabilization was only able to delay toxicity induced by nonfibrillar aggregates of Aβ1-42, but protected against higher concentrations of fibril-induced toxicity for 48 hours supports the literature that smaller aggregates exert a more toxic effect than their fibrillar counterparts [72,86,109].

Regardless of the MT state (disrupted vs. stabilized), neuronal stiffness significantly increased after exposure to Aβ1-42. This increase in stiffness can be related to the previous point that MT stabilization only delayed Aβ oligomer-induced toxicity compared to a more sustained protective effect against fibrillar aggregates. Studies have demonstrated that oligomeric Aβ1-42 aggregates caused higher stiffness in neurons than fibrillar Aβ1-42 [85]; therefore, Aβ1-42-induced increases in cell stiffness may be directly related to increased toxicity, as Aβ1-42 oligomers have been shown to produce a more toxic effect than fibrils [72,86,109]. The mechanism of increased neuronal stiffness can be explained by findings from model membranes and neuronal studies. When model membranes were exposed to Aβ1-40, the aggregates caused extensive membrane disruption and decreased the mechanical stiffness of the bilayer [110]. In neurons, a mechanical stiffening occurred after N2a neuroblastoma cells and HT22 hippocampal neurons were exposed to 5 μM oligomeric Aβ1-42 solutions for 30 minutes [85]. The observation of mechanical contrast between model membranes and whole cells after Aβ exposure is not unjustified, as mechanical measurements on cells account for the entire cell system rather than just the membrane. Thus, while the plasma membrane of a cell may become disrupted and less stiff after Aβ exposure, overall cell stiffening may be observed due to several factors, or a combination thereof. For example, Aβ aggregates may interact with the membrane thereby altering the fluidity or creating pores, which could increase intracellular osmotic pressure by unregulated ion influx [78,79,83–85]. Furthermore, studies have demonstrated that in primary hippocampal neurons, Aβ23-35 and Aβ1-42 (at concentrations greater than 5 μM) exposure stimulated the production of stress fibers through the activation of p38MAPK (mitogen-associated protein kinase) [111], which could also contribute to overall cell stiffening. Taken together, these findings demonstrate that Aβ-membrane interactions may reduce membrane stiffness while increasing the overall mechanical rigidity of neurons through a variety of mechanisms.

MT disruption, a consequence of the normal aging process, enhanced the toxicity of Aβ1-42 compared to neurons with unaltered or stabilized MTs. This has further pathological implications for the cell, as both synthetic and human-derived aggregates of Aβ1-42 stimulated Tau phosphorylation in a variety of cell cultures [26,112,113]. Additionally, in vivo studies have demonstrated that injection of Aβ1-42 aggregates into the brains of mice and rhesus monkeys caused Tau phosphorylation and the formation of NFTs [114,115]. Considering that the physiological role of Tau is to modulate MT assembly and stability, Aβ1-42 aggregate-induced phosphorylation disrupts the proper functioning of Tau thereby destabilizing MTs. This essentially creates a self-sustaining feedback mechanism, where age-related MT disruption enhances the toxic ability of Aβ1-42 aggregates to trigger the phosphorylation of Tau and further degrade MTs. This mechanism eventually causes synaptic dysfunction, neuronal death, and the breakdown of neuronal networks that leads to the clinical symptoms of AD. Given the evidence that MTs play such a critical role in AD pathology, MT stabilization has been explored as a potential treatment strategy [88,106,107,116–118]. Here, we found that treating neurons with the MT stabilizer, paclitaxel, delayed the onset of toxicity induced by nonfibrillar Aβ1-42 aggregates, which correlates well with studies demonstrating that MT stabilization has a more prolonged protective effect against Aβ1-42 fibrils.

5. Conclusion

We have provided evidence that altered MT networks influence a cell's ability to cope with exposure to oligomeric aggregates of Aβ1-42. While disrupting the MT network decreased the amount of Aβ that actually bound to cells, toxicity of Aβ was enhanced by destabilizing MT. In contrast, stabilizing MTs resulted in a protective effect. Regardless of the MT state (disrupted vs. stabilized vs. unaltered), exposure to Aβ1-42 aggregates resulted in cell stiffening. Our results demonstrate that MT modifications can have a direct influence on the toxicity of small Aβ1-42 aggregates.

Acknowledgments

This work was supported by NSF (CMMI1054211), and the Alzheimer's Association (NIRG-11-203834). N.S.-K. was supported by an NSF Integrative Graduate Education and Research Traineeship (DGE-1144676). The WVU Flow Cytometry Core Facility is supported by the MBRCC CoBRE grant (GM103488/RR032138), the Fortess S10 grant (OD016165) and the WV InBRE grant (GM103434). The BioNano Research Facility is supported by the NSF EPSCoR Research Infrastructure Improvement Cooperative Agreement (1003907), the state of West Virginia (WV EPSCoR via the Higher Education Policy Commission), and WVU.

Conflict of Interest

All authors declare no conflicts of interest in this paper.

References

1. Prokop A, Beaven R, Qu Y, et al. (2013) Using fly genetics to dissect the cytoskeletal machinery of neurons during axonal growth and maintenance. *J Cell Sci* 126: 2331–2341.
2. Iqbal K, Zaidi T, Wen G, et al. (1986) Defective brain microtubule assembly in Alzheimer's disease. *The Lancet* 328: 421–426.
3. Hirokawa N, Takeda S (1998) Gene targeting studies begin to reveal the function of neurofilament proteins. *J Cell Biol* 143: 1143–1143.
4. Riederer IM, Robert P, Porchet R, et al. (2003) Selective changes in the neurofilament and microtubule cytoskeleton of NF-H/LacZ mice. *J Neurosci Res* 71: 196–207.
5. Twelvetrees A, Hendricks AG, Holzbaur ELF (2012) SnapShot: Axonal Transport. *Cell* 149: 950–U251.
6. Elder GA, Friedrich VL, Margita A, et al. (1999) Age-related atrophy of motor axons in mice deficient in the mid-sized neurofilament subunit. *J Cell Biol* 146: 181–192.
7. Gourlay CW, Ayscough KR (2005) The actin cytoskeleton in ageing and apoptosis. *FEMS Yeast Res* 5: 1193–1198.
8. Gourlay CW, Carpp LN, Timpson P, et al. (2004) A role for the actin cytoskeleton in cell death and aging in yeast. *J Cell Biol* 164: 803–809.
9. Parhad IM, Scott JN, Cellars LA, et al. (1995) Axonal atrophy in aging is associated with a decline in neurofilament gene expression. *J Neurosci Res* 41: 355–366.

10. Raes M (1991) Involvement of microtubules in modifications associated with cellular aging. *Mutat Res* 256: 149–168.
11. Uchida A, Yorifuji H, Lee VMY, et al. (1999) Neurofilaments of aged rats: The strengthened interneurofilament interaction and the reduced amount of NF-M. *J Neurosci Res* 58: 337–348.
12. Vickers JC, Riederer BM, Marugg RA, et al. (1994) Alterations in neurofilament protein immunoreactivity in human hippocampal neurons related to normal aging and Alzheimers disease. *Neuroscience* 62: 1–13.
13. Bruusgaard JC, Liestøl K, Gundersen K (2006) Distribution of myonuclei and microtubules in live muscle fibers of young, middle-aged, and old mice. *J Appl Physiol* 100:2024–2030.
14. Raes M, Geuens G, de Brabander M, et al. (1983) Microtubules and microfilaments in ageing hamster embryo fibroblasts in vitro. *Exp Gerontol* 18: 241–254.
15. Raes M, Remacle J (1987) Alteration of the microtubule organization in aging WI-38 fibroblasts - a comparative study with embryonic hamster lung fibroblasts. *Exp Gerontol* 22: 47–58.
16. Saha S, Slepecky NB (2000) Age-related changes in microtubules in the guinea pig organ of Corti - Tubulin isoform shifts with increasing age suggest changes in micromechanical properties of the sensory epithelium. *Cell Tissue Res* 300: 29–46.
17. Neely MD, Sidell KR, Graham DG, et al. (1999) The lipid peroxidation product 4-hydroxynonenal inhibits neurite outgrowth, disrupts neuronal microtubules, and modifies cellular tubulin. *J Neurochem* 72: 2323–2333.
18. Cash AD, Aliev G, Siedlak SL, et al. (2003) Microtubule reduction in Alzheimer's disease and aging is independent of τ filament formation. *Am J Pathol* 162: 1623–1627.
19. Davies DC, Horwood N, Isaacs SL, et al. (1992) The effect of age and Alzheimer's disease on pyramidal neuron density in the individual fields of the hippocampal formation. *Acta Neuropathol* 83: 510–517.
20. Karbowski M, Spodnik JH, Teranishi M, et al. (2001) Opposite effects of microtubule-stabilizing and microtubule-destabilizing drugs on biogenesis of mitochondria in mammalian cells. *J Cell Sci* 114: 281–291.
21. Praprotnik D, Smith MA, Richey PL, et al. (1996) Filament heterogeneity within the dystrophic neurites of senile plaques suggests blockage of fast axonal transport in Alzheimer's disease. *Acta Neuropathol* 91: 226–235.
22. Terry RD, Katzman R (2001) Life span and synapses: will there be a primary senile dementia? *Neurobiol Aging* 22: 347–348.
23. Mattson MP, Magnus T (2006) Aging and neuronal vulnerability. *Nat Rev Neurosci* 7: 278–294.
24. Selkoe DJ (2011) Alzheimer's Disease. *Cold Spring Harb Perspect Biol* 3: a004457.
25. Zempel H, Thies E, Mandelkow E, et al. (2010) Aβ oligomers cause localized Ca2+ elevation, missorting of endogenous Tau into dendrites, Tau phosphorylation, and destruction of microtubules and spines. *J Neurosci* 30: 11938–11950.
26. De Felice FG, Wu D, Lambert MP, et al. (2008) Alzheimer's disease-type neuronal tau hyperphosphorylation induced by Aβ oligomers. *Neurobiol Aging* 29: 1334–1347.
27. Jin M, Shepardson N, Yang T, et al. (2011) Soluble amyloid β-protein dimers isolated from Alzheimer cortex directly induce Tau hyperphosphorylation and neuritic degeneration. *P Natl Acad Sci USA* 108: 5819–5824.

28. Busciglio J, Lorenzo A, Yeh J, et al. (1995) β-amyloid fibrils induce tau phosphorylation and loss of microtubule binding. *Neuron* 14: 879–888.
29. Ekinci FJ, Malik KU, Shea TB (1999) Activation of the L voltage-sensitive calcium channel by mitogen-activated protein (MAP) kinase following exposure of neuronal cells to β-amyloid - Map kinase mediates β-amyloid-induced neurodegeneration. *J Biol Chem* 274: 30322–30327.
30. Ferreira A, Lu Q, Orecchio L, et al. (1997) Selective phosphorylation of adult tau isoforms in mature hippocampal neurons exposed to fibrillar Aβ. *Mol Cell Neurosci* 9: 220–234.
31. Lorenzo A, Yankner BA (1994) β-amyloid neurotoxicity requires fibril formation and is inhibited by congo red. *P Natl Acad Sci USA* 91: 12243–12247.
32. Shea TB, Dergay AN, Ekinci FJ (1998) β-amyloid induced hyperphosphorylation of tau in human neuroblastoma cells involves map kinase. *Neurosc Res Commun* 22: 45–49.
33. Takashima A, Noguchi K, Sato K, et al. (1993) Tau protein kinase is essential for amyloid β protein induced neurotoxicity. *P Natl Acad Sci USA* 90: 7789–7793.
34. Cutler RG, Kelly J, Storie K, et al. (2004) Involvement of oxidative stress-induced abnormalities in ceramide and cholesterol metabolism in brain aging and Alzheimer's disease. *P Natl Acad Sci USA* 101: 2070–2075.
35. Nixon RA (2003) The calpains in aging and aging-related diseases. *Ageing Res Rev* 2: 407–418.
36. Stokin GB, Lillo C, Falzone TL, et al. (2005) Axonopathy and transport deficits early in the pathogenesis of Alzheimer's disease. *Science* 307: 1282–1288.
37. Mellon PL, Windle JJ, Goldsmith PC, et al. (1990) Immortalization of hypothalamic GNRH neurons by genetically targeted tumorigenesis. *Neuron* 5: 1–10.
38. Liposits Z, Merchenthaler I, Wetsel WC, et al. (1991) Morphological characterization of immortalized hypothalamic neurons synthesizing luteinizing hormone-releasing hormone. *Endocrinology* 129: 1575–1583.
39. Wetsel WC, Mellon PL, Weiner RI, et al. (1991) Metabolism of pro-luteinizing hormone releasing hormone in immortalized hypothalamic neurons. *Endocrinology* 129: 1584–1595.
40. Wetsel WC, Valenca MM, Merchenthaler I, et al. (1992) Intrinsic pulsatile secretory activity of immortalized luteinizing hormone releasing hormone secreting neurons. *P Natl Acad Sci USA* 89: 4149–4153.
41. Whyte DB, Lawson MA, Belsham DD, et al. (1995) A neuron specific enhancer targets expression of the gonadotropin releasing hormone gene to hypothalamic neurosecretory neurons. *Mol Endocrinol* 9: 467–477.
42. Stine WB, Dahlgren KN, Krafft GA, et al. (2003) In vitro characterization of conditions for amyloid-β peptide oligomerization and fibrillogenesis. *J Biol Chem* 278: 11612–11622.
43. Rheinlaender J, Geisse NA, Proksch R, et al. (2010) Comparison of scanning ion conductance microscopy with atomic force microscopy for cell imaging. *Langmuir* 27: 697–704.
44. Hutter JL, Bechhoefer J (1993) Calibration of atomic-force microscope tips. *Rev Sci Instrum* 64: 1868.
45. Burke KA, Godbey J, Legleiter J (2011) Assessing mutant huntingtin fragment and polyglutamine aggregation by atomic force microscopy. *Methods* 53: 275–284.
46. Simakova O, Arispe NJ (2007) The cell-selective neurotoxicity of the Alzheimer's amyloid-β peptide is determined by surface phosphatidylserine and cytosolic ATP levels. Membrane binding is required for amyloid-β toxicity. *J Neurosci* 27: 13719–13729.

47. Smiakova O, Arispe NJ (2011) Fluorescent Analysis of the Cell-Selective Alzheimer's Disease Amyloid-β Peptide Surface Membrane Binding: Influence of Membrane Components. *Int J Alzheimer's Dis* 2011: 917629.
48. Alenghat FJ, Nauli SM, Kolb R, et al. (2004) Global cytoskeletal control of mechanotransduction in kidney epithelial cells. *Exp Cell Res* 301: 23–30.
49. Rao S, Orr GA, Chaudhary AG, et al. (1995) Characterization of the taxol binding site on the microtubule: 2-(m-azidobenzoyl) taxol photolabels a peptide (amino acids 217-231) of β-tubulin. *J Biol Chem* 270: 20235–20238.
50. Dennerll TJ, Joshi HC, Steel VL, et al. (1988) Tension and compression in the cytoskeleton of PC-12 neurites II - quantative measurements. *J Cell Biol* 107: 665–674.
51. Joshi HC, Chu D, Buxbaum RE, et al. (1985) Tension and compression in the cytoskeleton of PC-12 neurites. *J Cell Biol* 101: 697–705.
52. Marx KA, Zhou T, Montrone A, et al. (2007) A comparative study of the cytoskeleton binding drugs nocodazole and taxol with a mammalian cell quartz crystal microbalance biosensor: Different dynamic responses and energy dissipation effects. *Anal Biochem* 361: 77–92.
53. Arborgh B, Bell P, Brunk U, et al. (1976) The osmotic effect of glutaraldehyde during fixation. A transmission electron microscopy, scanning electron microscopy and cytochemical study. *J Ultrastruct Res* 56: 339–350.
54. Braet F, Rotsch C, Wisse E, et al. (1998) Comparison of fixed and living liver endothelial cells by atomic force microscopy. *Appl Phys A-Mater* 66: S575.
55. Butt HJ, Wolff EK, Gould SAC, et al. (1990) Imaging cells with the atomic force microscope. *J Struct Biol* 105: 54–61.
56. Dulińska I, Targosz M, Strojny W, et al. (2006) Stiffness of normal and pathological erythrocytes studied by means of atomic force microscopy. *J Biochem Bioph Meth* 66: 1–11.
57. Kuznetsova TG, Starodubtseva MN, Yegorenkov NI, et al. (2007) Atomic force microscopy probing of cell elasticity. *Micron* 38: 824–833.
58. Le Grimellec C, Lesniewska E, Cachia C, et al. (1994) Imaging of the membrane surface of MDCK cells by atomic force microscopy. *Biophys J* 67: 36–41.
59. Lulevich V, Zink T, Chen H-Y, et al. (2006) Cell mechanics using atomic force microscopy-based single-cell compression. *Langmuir* 22: 8151–8155.
60. Mathur AB, Truskey GA, Monty Reichert W (2000) Atomic force and total internal reflection fluorescence microscopy for the study of force transmission in endothelial cells. *Biophys J* 78: 1725–1735.
61. Zachee P, Snauwaert J, Vandenberghe P, et al. (1996) Imaging red blood cells with the atomic force microscope. *Brit J Haematol* 95: 472–481.
62. Tsai MA, Waugh RE, Keng PC (1998) Passive mechanical behavior of human Neutrophils: effects of colchicine and paclitaxel. *Biophys J* 74: 3282–3291.
63. Rotsch C, Radmacher M (2000) Drug-induced changes of cytoskeletal structure and mechanics in fibroblasts: An atomic force microscopy study. *Biophys J* 78: 520–535.
64. Qiu H, Zhu Y, Sun Z, et al. (2010) Short Communication: Vascular smooth muscle cell stiffness as a mechanism for increased aortic stiffness with aging. *Circ Res* 107: 615–619.
65. Wu HW, Kuhn T, Moy VT (1998) Mechanical properties of L929 cells measured by atomic force microscopy: Effects of anticytoskeletal drugs and membrane crosslinking. *Scanning* 20: 389–397.

66. Hyo Il Jung Incheol S, Young Mok P, Ke Won K, et al. (1997) Colchicine activates actin polymerization by microtubule depolymerization. *Mol Cells* 7: 431–437.
67. Garland DL (1978) Kinetics and mechanism of colchicine binding to tubulin: evidence for ligand-induced conformational changes. *Biochemistry* 17: 4266–4272.
68. Spedden E, Staii C (2013) Neuron biomechanics probed by atomic force microscopy. *Int J Mol Sci* 14: 16124–16140.
69. Spedden E, White JD, Naumova EN, et al. (2012) Elasticity maps of living neurons measured by combined fluorescence and atomic force microscopy. *Biophys J* 103: 868–877.
70. Canale C, Seghezza S, Vilasi S, et al. (2013) Different effects of Alzheimer's peptide Aβ(1–40) oligomers and fibrils on supported lipid membranes. *Biophys Chem* 182: 23–29.
71. McLaurin J, Chakrabartty A (1996) Membrane disruption by Alzheimer β-amyloid peptides mediated through specific binding to either phospholipids or gangliosides: implications for neurotoxicity. *J Biol Chem* 271: 26482–26489.
72. Deshpande A, Mina E, Glabe C, et al. (2006) Different conformations of amyloid-β induce neurotoxicity by distinct mechanisms in human cortical neurons. *J Neurosci* 26: 6011–6018.
73. Blackley HKL, Sanders GHW, Davies MC, et al. (2000) In-situ atomic force microscopy study of β-amyloid fibrillization. *J Mol Biol* 298: 833–840.
74. Cizas P, Budvytyte R, Morkuniene R, et al. (2010) Size-dependent neurotoxicity of β-amyloid oligomers. *Arch Biochem Biophys* 496: 84–92.
75. Mastrangelo IA, Ahmed M, Sato T, et al. (2006) High-resolution atomic force microscopy of soluble Aβ42 oligomers. *J Mol Biol* 358: 106–119.
76. Reinert KC, Dunbar RL, Gao W, et al. (2004) Flavoprotein autofluorescence imaging of neuronal activation in the cerebellar cortex in vivo. *J Neurophysiol* 92:199–211.
77. Yates EA, Legleiter J (2014) Preparation Protocols of A beta(1-40) Promote the Formation of Polymorphic Aggregates and Altered Interactions with Lipid Bilayers. Biochemistry 53: 7038–7050.
78. Demuro A, Mina E, Kayed R, et al. (2005) Calcium Dysregulation and Membrane Disruption as a Ubiquitous Neurotoxic Mechanism of Soluble Amyloid Oligomers. *J Biol Chem* 280: 17294–17300.
79. Demuro A, Parker I, Stutzmann GE (2010) Calcium signaling and amyloid toxicity in Alzheimer disease. *J Biol Chem* 285: 12463–12468.
80. Kakio A, Nishimoto S-i, Yanagisawa K, et al. (2002) Interactions of amyloid β-protein with various gangliosides in raft-like membranes: importance of GM1 ganglioside-bound form as an endogenous seed for Alzheimer amyloid. *Biochemistry* 41: 7385–7390.
81. Kayed R, Sokolov Y, Edmonds B, et al. (2004) Permeabilization of lipid bilayers is a common conformation-dependent activity of soluble amyloid oligomers in protein misfolding diseases. *J Biol Chem* 279: 46363–46366.
82. Kremer JJ, Pallitto MM, Sklansky DJ, et al. (2000) Correlation of β-amyloid aggregate size and hydrophobicity with decreased bilayer fluidity of model membranes. *Biochemistry* 39: 10309–10318.
83. Mattson MP, Chan SL (2003) Neuronal and glial calcium signaling in Alzheimer's disease. *Cell Calcium* 34: 385–397.
84. Quist A, Doudevski I, Lin H, et al. (2005) Amyloid ion channels: A common structural link for protein-misfolding disease. *P Natl Acad Sci USA* 102: 10427–10432.

85. Lulevich V, Zimmer CC, Hong H-s, et al. (2010) Single-cell mechanics provides a sensitive and quantitative means for probing amyloid-β peptide and neuronal cell interactions. *P Natl Acad Sci USA* 107: 13872–13877.
86. Choi YJ, Chae S, Kim JH, et al. (2013) Neurotoxic amyloid-β oligomeric assemblies recreated in microfluidic platform with interstitial level of slow flow. *Sci Rep* 3:1921.
87. Lin H, Bhatia R, Lal R (2001) Amyloid-β protein forms ion channels: implications for Alzheimer's disease pathophysiology. *FASEB J* 15: 2433–2444.
88. Michaelis ML, Ansar S, Chen Y, et al. (2005) β-amyloid-induced neurodegeneration and protection by structurally diverse microtubule-stabilizing agents. *J Pharmocol Exp Ther* 312: 659–668.
89. Piccini A, Russo C, Gliozzi A, et al. (2005) β-amyloid Is different in normal aging and in Alzheimer disease. *J Biol Chem* 280: 34186–34192.
90. Walsh DM, Hartley DM, Kusumoto Y, et al. (1999) Amyloid β-protein fibrillogenesis - Structure and biological activity of protofibrillar intermediates. *J Biol Chem* 274: 25945–25952.
91. Anesti V, Scorrano L (2006) The relationship between mitochondrial shape and function and the cytoskeleton. *BBA-Bioenergetics* 1757: 692–699.
92. Ball EH, Singer SJ (1982) Mitochondria are associated with microtubules and not with intermediate filaments in cultured fibroblasts. *P Natl Acad Sci USA* 79: 123–126.
93. Fuchs F, Prokisch H, Neupert W, et al. (2002) Interaction of mitochondria with microtubules in the filamentous fungus Neurospora crassa. *J Cell Sci* 115: 1931–1937.
94. Heggeness MH, Simon M, Singer SJ (1978) Association of mitochondria with microtubules in cultured cells. *P Natl Acad Sci USA* 75: 3863–3866.
95. Shahpasand K, Uemura I, Saito T, et al. (2012) Regulation of mitochondrial transport and inter-microtubule spacing by Tau phosphorylation at the sites hyperphosphorylated in Alzheimer's disease. *J Neurosci* 32: 2430–2441.
96. De Brabander MJ, Van de Velre RML, Aerts FEM, et al. (1976) The effects of methyl [5-(2-thienylcarbonyl)-1H-benzimidazol-2-yl]carbamate, (R 17934; NSC 238159), a new synthetic antitumoral drug interfering with microtubules, on mammalian cells cultured in vitro. *Cancer Res* 36: 905–916.
97. Bryan J (1972) Vistabline and microtubules: Definition of 3-classes of binding-sites in isolated microtubule crystals. *Biochemistry* 11: 2611–2616.
98. Hoebeke J, Vannijen G, Debrabander M (1976) Interaction of oncodazole (R17934), new anti-tumoral drug, with rat brain tubulin. *Biochem Biophys Res Co* 69: 319–324.
99. Owellen RJ, Owens AH, Donigian DW (1972) Binding of vincristine, vistabline and colchicine to tubulin. *Biochem Biophys Res Co* 47: 685.
100. Ringel I, Sternlicht H (1984) C-13 NMR study of microtubule protein- evidence for a 2nd colchicine site involved in the inhibition of microtubule assembly. *Biochemistry* 23: 5644–5653.
101. Williams RF, Aivaliotis MJ, Barnes LD, et al. (1983) High performance liquid-chromatographic application of the Hummel and Dreyer method for the determination of colchicine-tubulin binding parameters. *J Chromatogr* 266: 141–150.
102. Xu K, Schwarz PM, Luduena RF (2002) Interaction of nocodazole with tubulin isotypes. *Drug Develop Res* 55: 91–96.

103. Head J, Lee LLY, Field DJ, et al. (1985) Equilibrium and rapid kinetic studies on nocodazole-tubulin interaction. *J Biol Chem* 260: 1060–1066.
104. Samson F, Donoso JA, Hellerbettinger I, et al. (1979) Nocodazole action on tubulin assembly, axonal ultrastructure and fast axoplasmic transport. *J Pharmacol Exp Ther* 208: 411–417.
105. Zieve GW, Turnbull D, Mullins JM, et al. (1980) Production of large numbers of mitotic mammalian cells by use of the reversible microtubule inhibitor nocodazole- nocodazole accumulated mitotic cells. *Exp Cell Res* 126: 397–405.
106. Michaelis ML, Ranciat N, Chen Y, et al. (1998) Protection against β-amyloid toxicity in primary neurons by paclitaxel (Taxol). *J Neurochem* 70: 1623–1627.
107. Michaelis ML, Chen YX, Hill S, et al. (2002) Amyloid peptide toxicity and microtubule-stabilizing drugs. *J Mol Neurosci* 19: 101–105.
108. Nilsson MR (2004) Techniques to study amyloid fibril formation in vitro. *Methods* 34: 151–160.
109. Dahlgren KN, Manelli AM, Stine WB, et al. (2002) Oligomeric and fibrillar species of amyloid-β peptides differentially affect neuronal viability. *J Biol Chem* 277: 32046–32053.
110. Burke KA, Yates EA, Legleiter J (2013) Amyloid-forming proteins alter the local mechanical properties of lipid membranes. *Biochemistry* 52: 808–817.
111. Song C, Perides G, Wang D, et al. (2002) β-Amyloid peptide induces formation of actin stress fibers through p38 mitogen-activated protein kinase. *J Neurochem* 83: 828–836.
112. Ma Q-L, Yang F, Rosario ER, et al. (2009) β-amyloid oligomers induce phosphorylation of Tau and inactivation of insulin receptor substrate via c-Jun N-terminal kinase signaling: suppression by omega-3 fatty acids and curcumin. *J Neurosci* 29: 9078–9089.
113. Esposito G, De Filippis D, Carnuccio R, et al. (2006) The marijuana component cannabidiol inhibits β-amyloid-induced tau protein hyperphosphorylation through Wnt/β-catenin pathway rescue in PC12 cells. *J Mol Med* 84: 253–258.
114. Geula C, Wu CK, Saroff D, et al. (1998) Aging renders the brain vulnerable to amyloid β-protein neurotoxicity. *Nat Med* 4: 827–831.
115. Götz J, Chen F, van Dorpe J, et al. (2001) Formation of neurofibrillary tangles in P301L Tau transgenic mice induced by Aβ42 fibrils. *Science* 293: 1491–1495.
116. Ballatore C, Brunden KR, Huryn DM, et al. (2012) Microtubule Stabilizing Agents as Potential Treatment for Alzheimer's Disease and Related Neurodegenerative Tauopathies. *J Med Chem* 55: 8979–8996.
117. Lee VMY, Daughenbaugh R, Trojanowski JQ (1994) Microtubule stabilizing drugs for the treatment of Alzheimer's disease. *Neurobiol Aging* 15: S87–S89.
118. Zhang B, Carroll J, Trojanowski JQ, et al. (2012) The microtubule-stabilizing agent, epothilone D, reduces axonal dysfunction, neurotoxicity, cognitive deficits, and Alzheimer-like pathology in an interventional study with aged Tau transgenic mice. *J Neurosci* 32: 3601–3611.

AIMS Press